Two-color laser ionization injection

L.-L. Yu,[1,2,3] E. Esarey,[1] C. B. Schroeder,[1] J.-L. Vay,[1]
C. Benedetti,[1] C. G. R. Geddes,[1] M. Chen,[3] and W. P. Leemans[1,2]

[1]*Lawrence Berkeley National Laboratory, Berkeley, California 94720, USA*
[2]*Department of Physics, University of California, Berkeley, California 94720, USA*
[3]*Key Laboratory for Laser Plasmas (Ministry of Education), Department of Physics and Astronomy, Shanghai Jiao Tong University, Shanghai 200240, China*

(Dated: February 25, 2014)

A method is proposed to generate femtosecond, ultra-low emittance ($\sim 10^{-8}$ m rad), electron beams in a laser-plasma accelerator using two lasers of different colors. A long-wavelength pump pulse, with large ponderomotive force and small peak electric field, excites a wake without fully ionizing a high-Z gas. A short-wavelength injection pulse, with small ponderomotive force and large peak electric field, co-propagating and delayed with respect to the pump laser, ionizes a fraction of the remaining bound electrons at a trapping wake phase, generating an electron beam that is accelerated in the wake.

In laser-driven plasma-based accelerators [1], the accelerating and focusing fields (wakefields) are driven by the ponderomotive force of the laser pulse $F \simeq -m_e c^2 \nabla a^2/2$, where $a = eA/m_e c^2$ is the normalized amplitude of the laser vector potential, c is the speed of light, and e and m_e are the electron charge and mass, respectively. For a resonant laser pulse with $a \sim 1$, the accelerating field is on the order of $E_p(\mathrm{V/m}) \simeq 96\sqrt{n_0(\mathrm{cm}^{-3})}$, with n_0 the plasma electron density, and E_p can be several orders of magnitude greater than the fields in conventional accelerators. In addition, laser-plasma accelerators have the potential to produce extremely short electron beams with durations $\tau_b < \lambda_p/c$, where $\lambda_p(\mu\mathrm{m}) \simeq 3.3 \times 10^{10}/\sqrt{n_0(\mathrm{cm}^{-3})}$ is the plasma wavelength. High-quality GeV electron beams were first demonstrated using an intense laser interacting in a cm-scale plasma, relying on self-injection for electron beam generation [2]. In the nonlinear laser-driven bubble regime, where the particles are self-trapped, simulations and experiments show that an electron beam with $\sigma_x \sim 0.1$ μm, $\sigma_{p_x}/(m_e c) \sim 1$, and $\epsilon_n \sim 0.1$ mm mrad can be achieved [3], where σ_x is the root-mean-square (rms) beam radius, $\sigma_{p_x}/(m_e c)$ is the normalized rms transverse momentum, and the normalized transverse emittance can be estimated as $\epsilon_n \simeq \sigma_x \sigma_{p_x}/(m_e c)$. High-quality, laser-plasma-accelerated electron beams could be good candidates to drive free-electron lasers, enabling a new generation of low-cost, compact light sources [4, 5]. Improved beam phase space characteristics, and, in particular, reduced transverse emittance, is highly desired for light sources and other applications.

In order to improve the quality and stability of laser-plasma-accelerated electron beams, controlled injection methods are actively being pursued, including colliding pulse injection [6, 7], plasma density transitions [8, 9], and ionization injection [10–15]. Ionization injection, compared to self-trapping, allows electron beam generation at lower plasma densities and, hence, higher beam energies can be achieved. In conventional ionization injection into laser-plasma accelerators [12–14], a single laser pulse is used both for wake generation and high-Z gas ionization. Typically $a_0 \gtrsim 2$, with $w_0 \sim 10$ μm, is needed to excite a sufficiently large wake so that an electron ionized near the peak intensity of the laser pulse can be on a trapped orbit, where w_0 is the laser spot size and a_0 is the peak normalized amplitude of the laser vector potential [14]. For linear polarization, $a_0^2 = 7.3 \times 10^{-19}[\lambda(\mu\mathrm{m})]^2 I_0(\mathrm{W/cm}^2)$ with I_0 the peak laser intensity and λ the laser wavelength in vacuum. Using ionization injection the emittance grows with increasing ionization laser intensity $\epsilon_n \propto a_0$. Since $a_0 \gtrsim 2$ is required for electron trapping [14], reducing the injected beam emittance using single-pulse ionization injection is limited. One variant on ionization injection is to use a beam-driven plasma wake in the blow-out regime, followed by a laser pulse to trap electrons via ionization injection, and simulations of this method indicate that ultra-low emittance beams can be generated [16, 17]. Since field ionization by the beam-driver can be small, this reduces the intensity required ($\sim \mathrm{PW/cm}^2$) for the ionizing laser.

In this Letter we propose an all-optical, two-pulse, two-color, laser-ionization injection method to generate low-emittance, high-quality electron beams in a laser-plasma accelerator. This injection method relies on two co-propagating laser pulses in a high-Z gas: a pump pulse with a long laser wavelength for wakefield generation and a delayed injection pulse with a short laser wavelength for ionization injection. Since the peak field of the laser is $E = (2\pi m_e c^2/e)a/\lambda$, the long wavelength pump laser can drive a large wakefield (large a) with a small peak field such that some electrons remain atomically bound (typically inner-shell electrons). The delayed short wavelength injection laser can, conversely, have a large peak laser field to ionize electrons into trapped orbits with a small quiver momentum (small a to reduce the emittance of the trapped beam). This all-optical system generates ultra-low emittance beams, while offering the advantages

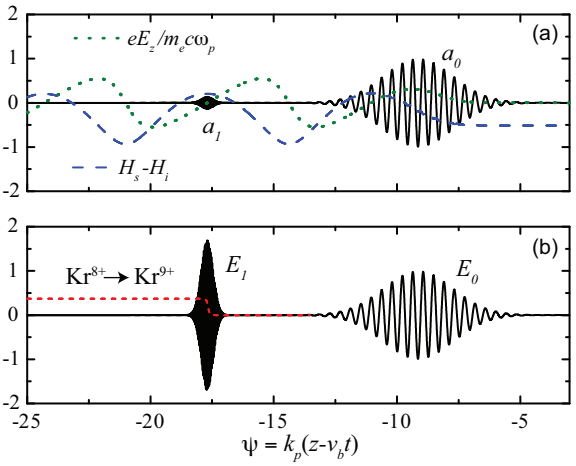

FIG. 1. (Color online) Example of two-color laser-ionization injection using Kr gas. (a) The vector potentials of the pump pulse a_0 (with $\lambda_0 = 5$ μm) and injection pulse a_1 (with $\lambda_1 = 0.4$ μm) (black curves) and the normalized excited wakefield $eE_z/(m_e k_p c^2)$ (green dotted curve). $H_s - H_i$ is shown as a function of wake phase ψ (blue dashed curve), and $H_s - H_i > 0$ is the trapping condition for an ionized electron. (b) The electric fields of the pump pulse E_0 and injection pulse E_1 (black curves), normalized to the peak of E_0, and the fraction of ionization for $Kr^{8+} \rightarrow Kr^{9+}$ (red dashed curve).

of compactness, simplicity, and synchronization (if the two color lasers are derived from a single laser oscillator).

This injection concept is illustrated in Fig. 1. In this example, a long-wavelength ($\lambda_0 = 5$ μm) pump pulse with an amplitude $a_0 = 1$ propagates in a Kr gas, ionizes the Kr to Kr^{8+}, and excites a large wake. The electric field of the pump pulse E_0 is sufficiently low, because of the long laser wavelength, so that it can not ionize the 9th electron of Kr (ionization potential 230 eV). A short-wavelength ($\lambda_1 = 0.4$ μm) injection pulse with an amplitude $a_1 = 0.135$ is co-propagating, delayed behind the pump laser, and ionizes the 9^{th} electron of Kr owing to the higher peak electric field $E_1 > E_0$. The fraction of Kr^{9+} produced is shown in Fig. 1(b) (dashed red curve). The injection pulse can be delayed with respect to the pump laser such that it is located at a wake phase where the separatrix orbit has negative momentum, and electrons ionized at rest will be on trapped orbits. In order to achieve a small beam transverse emittance, it is desirable that the amplitude a_1 be as small as possible, while producing sufficient beam charge. As described below, two-dimensional (2D) particle-in-cell (PIC) simulations show, for an example using Kr gas, an injected electron beam with rms transverse emittance of $\sim$0.03 mm mrad is generated. This is an order of magnitude smaller than previously achieved in laser-plasma accelerators [3].

The electron motion in the plasma wake can be described using a Hamiltonian approach [1]. The one-dimensional (1D) Hamiltonian describing the electron orbits, behind the pump pulse, is $H(u_z, \psi) = (1 + u_z^2)^{1/2} - \beta_p u_z - \phi(\psi)$, where $\psi = k_p \xi$ is the wake phase with $k_p = 2\pi/\lambda_p$ the plasma wavenumber, $\xi = z - v_p t$ is forward co-moving coordinate, $u_z = p_z/m_e c$ is the normalized longitudinal momentum of the electron, $\phi(\psi) = e\Phi/mc^2$ is the normalized wake potential, and $\beta_p = v_p/c$ is the normalized wake phase velocity. In an underdense plasma ($\lambda_p \gg \lambda_0 > \lambda_1$), $\beta_p \simeq 1$. The excited normalized wakefield is $eE_z/(m_e k_p c^2) = -k_p^{-1} \partial\phi/\partial\xi$. The quiver motion and wake excited from the injection pulse may be neglected since $a_1^2 \ll a_0^2 \sim 1$. The 1D separatrix (the boundary between trapped and untrapped orbits) is given by $u_s = u_z(H_s(\gamma_p, \psi_{\min}))$, where $\gamma_p = (1-\beta_p^2)^{-1/2}$, $\phi(\psi_{\min}) = \phi_{\min}$ is the minimum wake potential amplitude, and $H_s = 1/\gamma_p - \phi_{\min}$. A three-dimensional (3D) separatrix may be defined by trapped and focused orbits and has $H_{s,3D} = 1/\gamma_p$ [6]. For an electron ionized in the wake by the injection pulse, the orbit is described by $H(u_z, \psi) = H_i = 1 - \phi(\psi_i)$ [14], assuming that the electron is ionized at rest and $a_1^2 \ll 1$, where ψ_i is the wake phase at ionization. The trapping condition for the ionized electron is $H_s - H_i > 0$, and the optimal injection phase occurs where $H_s - H_i$ is maximum, as shown in Fig. 1(a). For example, if we consider a $\lambda_0 = 5$ μm pump laser pulse, circularly polarized with a Gaussian profile $a_0(\xi) = a_0 \exp(-\xi^2/L_0^2)$ and $k_p L_0 = 2$ (to maximize the wake excitation), in a plasma with $n_0 = 2 \times 10^{17}$ cm^{-3} ($\lambda_p = 75$ μm), then the intensity threshold of the pump pulse for trapping at the optimal injection phase is $a_{0,\text{th}} = 0.88$ in 1D and $a_{0,\text{th}} = 1.14$ in 3D. This is the pump laser intensity to drive a wake large enough such that a particle at rest, at the proper wake phase, is trapped. A circularly-polarized pump pulse is advantageous since it generates a larger ponderomotive force for a given peak laser field, compared to linear-polarization (by a factor of 2). In this example, the ionization rate of $Kr^{8+} \rightarrow Kr^{9+}$ for the circularly-polarized pump pulse ($a_0 = 1$ and $\lambda_0 = 5$ μm) is more than two orders of magnitude smaller than that for a linearly-polarized pump pulse producing the same wake (requiring $a_0 = \sqrt{2}$).

A linearly-polarized injection pulse with a short wavelength can have a large laser electric field $E_1 > E_0$, achieving a high ionization rate, and a small laser vector potential $a_1 \ll a_0$ to reduce the ionization induced emittance. The injection pulse can be delayed to locate it at the optimal wake phase in the second bucket of the wake. An example of this is shown in Fig. 1(b), where $Kr^{8+} \rightarrow Kr^{9+}$ is ionized using an injection pulse with $\lambda_1 = 0.4$ μm and $a_1 = 0.135$. Since the ionization region occupies a small fraction of wake phase, due to the short injection pulse duration, all ionized electrons satisfy the trapping condition and are trapped in the wake.

The normalized transverse momentum of the ionized electron is $u_\perp(\psi) = p_\perp/m_e c \simeq a_{1,\perp}(\psi) - a_{1,\perp}(\psi_i)$. Al-

though most of the electrons are ionized near the peak laser electric field, where the ionization probability is largest, and $a_{1,\perp}(\psi_i) \simeq 0$, some of the electrons are ionized off-peak with a finite $a_{1,\perp}(\psi_i)$. After ionization, the electron slips through the injection laser pulse and is trapped behind the laser pulse, i.e., $a_{1,\perp}(\psi) = 0$, then the transverse momentum gained by the electron in the injection laser pulse is $u_\perp(\psi) = -a_{1,\perp}(\psi_i)$. This residual transverse momentum, resulting from the electron being ionized off-peak of the laser electric field, contributes to the initial beam emittance. The beam transverse emittance is also determined by the transverse wakefield. Electrons ionized off-axis transversely are accelerated by the transverse wakefield. The condition for a matched beam radius is $\sigma_{x,m} = (\epsilon_n/\gamma k_\beta)^{1/2}$, where γ is the relativistic factor of the beam and k_β is the betatron wavenumber that is related to the wake focusing force, $\gamma k_\beta^2 x \simeq k_p(E_x - B_y)/E_p$ for a relativistic beam and $x \ll w_0$. Note that we are considering a wake in the quasi-linear regime $a_0 \sim 1$, below the amplitude required for electron cavitation, so that $k_\beta < k_p/\sqrt{2\gamma}$. Using two-color laser-ionization injection, the beam radius can be made small enough to satisfy the matching condition $\sigma_x \sim \sigma_{x,m}$ due to the narrow transverse ionization region of the tightly-focused ionization pulse.

The two-color laser-ionization injection technique was examined with 2D PIC simulations using the code WARP [18], where the direct-current tunneling ionization model [19, 20] is implemented. For the numerical example considered, the Keldysh parameter is small and tunneling ionization is dominant [19]. Since $a_1 \ll 1$ and $\lambda_1^2 \ll \lambda_0^2 \ll \lambda_p^2$, the nonlinear feedback of the plasma on the injection pulse is negligible during the simulated interaction time. Therefore, in order to save computational time, the short-wavelength injection pulse was not solved on the computational grid but was added analytically onto the macro-particles (assuming a paraxial evolution of the injection laser pulse in the plasma). The temporal resolution was $dt = 0.047\tau_1$, where τ_1 is a laser cycle of the injection pulse, which was found to be sufficient to accurately model the ionization process. The simulation box size was 276 μm$\times$215 μm with two macro-particles per cell. The resolution of the computational grid was $\Delta z = 0.08$ μm and $\Delta x = 0.18$ μm. A mixed gas (high-Z and low-Z) was used for the ionization injection region followed by a long region of a low-Z gas for the post-acceleration without additional trapping. This two-region gas structure allows control of the injection number and energy spread by changing the gas composition, concentration, and length of the mixed gas region [14]. The ionization injection region is also determined by the Rayleigh range of the injection pulse $Z_{R,1} = \pi w_1^2/\lambda_1$, and the Rayleigh range may be used to control (limit) the effective length of the ionization injection region [15]. The electron density (after ionization by the pump laser) is fixed to $n_0 = n_e + 8n_{\rm Kr} = 2 \times 10^{17}$ cm^{-3}, where

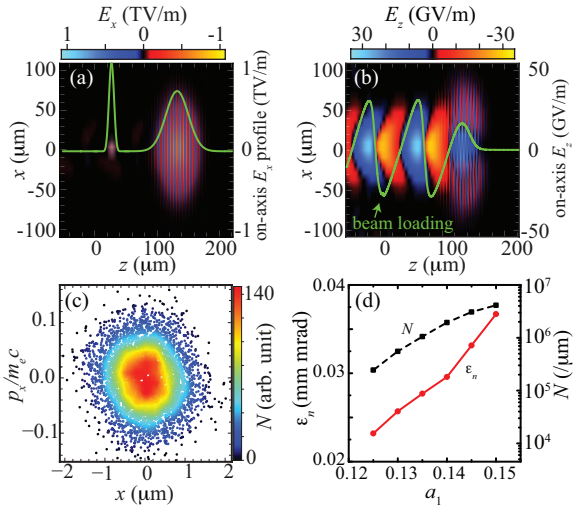

FIG. 2. (Color online) (a) The electric field of the laser pulses (green curve is on-axis laser field profile), (b) the longitudinal wakefield (green curve is on-axis wakefield), and (c) the transverse phase space of the injected electrons, after the (mixed gas) ionization injection region. (d) The normalized transverse emittance ϵ_n (red solid curve) and trapped electron number N (black dashed curve) versus the injection pulse amplitude a_1. See text for laser-plasma parameters.

n_e electron density produced by ionization of the low-Z gas (e.g., H gas), and the pump laser ionizes the Kr gas to Kr^{8+}. The total electron density n_0 is fixed so that density ramp effects are negligible. The concentration of the Kr gas in the simulations is set to $n_{\rm Kr} = 0.1n_0$. The Kr gas region is trapezoid-shaped starting at $z = -100$ μm and ending at $z = 0$, with a plateau of 50 μm. The pump and injection pulses have Gaussian profiles $a(\xi)_{0,1} = a_{0,1}\exp[-(\xi - \xi_{0,1})^2/L_{0,1}^2]$, with amplitudes $a_0 = 1.17$ and $a_1 = 0.135$, wavelengths $\lambda_0 = 5$ μm and $\lambda_1 = 0.4$ μm, durations (FWHM) $T_0 = 92$ fs and $T_1 = 16$ fs, and spot sizes $w_0 = 36$ μm and $w_1 = 5$ μm, respectively. The peak of the injection pulse is located at the optimal injection wake phase in the second bucket of the wake, which is delayed by $|\xi_0 - \xi_1| = 106.25$ μm from the peak of the pump pulse.

Figure 2 shows the PIC simulation results of the two-color laser-ionization injection for these laser-plasma parameters after the injection pulse propagates to the end of the Kr gas region. The electron beam is in the second wake bucket. The ionized electron number is $1.05 \times 10^6/\mu$m, and all the ionized electrons are on trapped orbits in the wake (in agreement with the analytical prediction). Figure 2(c) shows the transverse phase space of the ionized electrons. Most of the electrons are ionized at the peak of the injection laser electric field, with zero residual transverse momentum. Electrons ionized off-peak of the laser field are trapped and obtain finite transverse momentum. The maximum momentum is $p_x/m_e c \simeq 0.17$,

which is larger than the vector potential amplitude a_1 due to the effects of the transverse force of the wakefield and transverse ponderomotive force of the injection laser pulse. The rms beam radius and transverse momentum are $\sigma_x = 0.55\ \mu\text{m} \simeq 0.1 w_0$ and $\sigma_{p_x}/(m_e c) = 0.05$, respectively. Here σ_{p_x} is an order of magnitude smaller than that observed in simulations of single-pulse ionization injection [14]. For the beam in Fig. 2(c) the transverse emittance is $\epsilon_n = 0.028$ mm mrad. Note that the maximum focusing field on the beam is $F/e = 2.3$ GV/m, which is an order of magnitude smaller than the accelerating field. This smaller focusing force reduces the transverse momentum gained from the wake potential and allows matched propagation.

Figure 3(a) shows the maximum beam energy versus the acceleration distance. The energy increases approximately linearly since the propagation distance ($z = 1.8$ mm) is less than a dephasing length. Note that the wakefield amplitude is locally suppressed by beam loading, as shown in Figure 2(b). The rms beam length is $\sigma_z = 0.9\ \mu$m. The pump pulse can be guided in a plasma channel and propagate several Rayleigh lengths ($Z_{R,0} = 0.8$ mm) with minimum laser evolution if matched to the channel [21]. The maximum energy of the beam after a dephasing length can be estimated as $W_{\max} \simeq (2/\pi) e E_{z,\max} L_d = 315$ MeV, where $L_d = \lambda_p^3/\lambda_0^2 \simeq 17$ mm is the dephasing length. Note that use of a longer wavelength laser for driving the wake results in a shorter dephasing length. The energy spectra are shown in Fig 3(b) at different acceleration distances $z = 0.6$ mm, 1.2 mm, and 1.8 mm. The relative energy spread is $\sigma_\gamma/\langle\gamma\rangle = 0.025$ at $z = 1.8$ mm. For these short electron beams with mild beam loading, additional acceleration will increase of the mean beam energy and the relative energy spread will further decrease. For a mismatched beam, the beam energy spread may lead to betatron phase mixing and emittance growth on the scale length $\sim 2\pi k_\beta^{-1}(\langle\gamma\rangle/\sigma_\gamma)$.

The beam transverse emittance evolution is shown in Fig. 3(a). The emittance can be controlled by changing the injection pulse amplitude a_1 or the spot size w_1. As shown in Fig. 2(d), decreasing the injection pulse amplitude a_1 reduces the emittance; however, fewer electrons are ionized and trapped. The charge increases linearly with increasing concentration of the Kr gas (up to the beam loading limit) [14]. Increasing the ionization pulse duration will also increase the fraction of ionization and hence the trapped charge (provided the electrons are ionized at a trapped phase of the wake) without significantly increasing the emittance, for $k_p L_1 \ll 1$ (this is in agreement with Ref. [17]). The length of the Kr gas region may also be increased for generation of additional trapped charge, however, ionization decreases rapidly due to the laser diffraction after a Rayleigh length of the ionization pulse ($Z_{R,1} = 0.2$ mm for the example considered). The Rayleigh length of the injection pulse may also be used

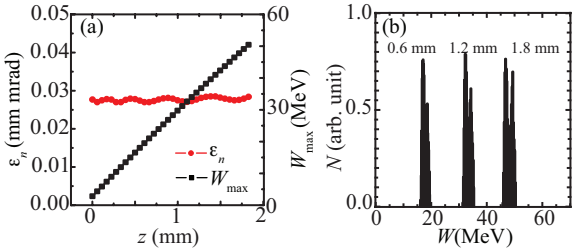

FIG. 3. (Color online) (a) The normalized transverse emittance ϵ_n, and the maximum energy $W_{\max}$ of the trapped electron beam versus acceleration distance z. (b) Electron beam energy spectra at $z = 0.6$ mm, 1.2 mm, and 1.8 mm. The laser-plasma parameters are the same as Fig. 2.

to control the ionization injection region [15].

In summary, we have proposed a method for generation of femtosecond, ultra-low emittance ($\sim 10^{-8}$ m rad), electron beams in a laser-plasma accelerator using two laser pulses of different colors. A long-wavelength pump pulse (with large ponderomotive force and small peak laser electric field) excites a large plasma wake without fully ionizing a high-Z gas, and a short-wavelength injection pulse (with small ponderomotive force and large peak laser electric field) co-propagating and delayed with respect to the pump laser, ionizes a fraction of the remaining bound electrons of the high-Z gas at a trapping wake phase, generating an electron beam that is accelerated in the wakefield. This method can produce electron beams with an order of magnitude smaller transverse emittance compared to single pulse ionization injection, e.g., $\epsilon_n \sim 0.03$ mm mrad for the example considered above. Other laser wavelengths and gases could be envisioned that may be more optimized. The emittance is determined by amplitude of the ionizing laser $\epsilon_n \propto a_1$. Thus, by controlling the amplitude of the injection pulse, the emittance can be controlled. Although this study considered a quasi-linear wake regime, the two-color ionization injection method can be applied to the nonlinear bubble regime, which may have additional advantages.

This method of injection would benefit from development of optical parametric chirped-pulse amplification laser systems [22] that can deliver high power, short pulse lasers with great wavelength flexibility, and be seeded by a single laser system (e.g., with a Ti:sapphire oscillator providing phase stabilization) for synchronization. A first experimental test could be done with a simple frequency-doubled (e.g., Ti:sapphire, 0.4 μm) injection pulse delayed with respect to a (0.8 μm) pump pulse. In this case one can consider lower injection laser intensity $a_1 \sim a_0 \lambda_1/\lambda_0$, and a corresponding reduction in beam emittance.

The authors would like to thank S. Bulanov, S. Rykovanov, J. van Tilborg, Cs. Toth, Zhengming Sheng, and Liejia Qian for discussions. This work was supported

by the Director, Office of Science, Office of High Energy Physics, of the U.S. Department of Energy under Contract No. DE-AC02-05CH11231 and by the National Science Foundation under Grant No. PHY-0935197. Computational resources of the National Energy Research Scientific Computing Center were used.

[1] E. Esarey, C. B. Schroeder, and W. P. Leemans, Rev. Mod. Phys. **81**, 1229 (2009).

[2] W. P. Leemans, B. Nagler, A. J. Gonsalves, C. Tóth, K. Nakamura, C. G. R. Geddes, E. Esarey, C. B. Schroeder, and S. M. Hooker, Nature Phys. **2**, 696 (2006).

[3] G. R. Plateau, C. G. R. Geddes, D. B. Thorn, M. Chen, C. Benedetti, E. Esarey, A. J. Gonsalves, N. H. Matlis, K. Nakamura, C. B. Schroeder, S. Shiraishi, T. Sokollik, J. van Tilborg, C. Toth, S. Trotsenko, T. S. Kim, M. Battaglia, T. Stöhlker, and W. P. Leemans, Phys. Rev. Lett. **109**, 064802 (2012); R. Weingartner, S. Raith, A. Popp, S. Chou, J. Wenz, K. Khrennikov, M. Heigoldt, A. R. Maier, N. Kajumba, M. Fuchs, B. Zeitler, F. Krausz, S. Karsch, and F. Grüner, Phys. Rev. ST Accel. Beams **15**, 111302 (2012).

[4] H.-P. Schlenvoigt, K. Haupt, A. Debus, F. Budde, O. Jäckel, S. Pfotenhauer, H. Schwoerer, E. Rohwer, J. G. Gallacher, E. Brunetti, R. P. Shanks, S. M. Wiggins, and D. A. Jaroszynski, Nature Phys. **4**, 130 (2008); M. Fuchs, R. Weingartner, A. Popp, Z. Major, S. Becker, J. Osterhoff, I. Cortrie, B. Zeitler, R. Hörlein, G. D. Tsakiris, U. Schramm, T. P. Rowlands-Rees, S. M. Hooker, D. Habs, F. Krausz, S. Karsch, and F. Grüner, *ibid.* **5**, 826 (2009).

[5] A. R. Maier, A. Meseck, S. Reiche, C. B. Schroeder, T. Seggebrock, and F. Grüner, Phys. Rev. X **2**, 031019 (2012); Z. Huang, Y. Ding, and C. B. Schroeder, Phys. Rev. Lett. **109**, 204801 (2012).

[6] E. Esarey, R. F. Hubbard, W. P. Leemans, A. Ting, and P. Sprangle, Phys. Rev. Lett. **79**, 2682 (1997); C. B. Schroeder, P. B. Lee, J. S. Wurtele, E. Esarey, and W. P. Leemans, Phys. Rev. E **59**, 6037 (1999); G. Fubiani, E. Esarey, C. B. Schroeder, and W. P. Leemans, *ibid.* **70**, 016402 (2004); H. Kotaki, S. Masuda, M. Kando, J. K. Koga, and K. Nakajima, Phys. Plasmas **11**, 3296 (2004).

[7] J. Faure, C. Rechatin, A. Norlin, A. Lifschitz, Y. Glinec, and V. Malka, Nature **444**, 737 (2006); C. Rechatin, J. Faure, A. Ben-Ismail, J. Lim, R. Fitour, A. Specka, H. Videau, A. Tafzi, F. Burgy, and V. Malka, Phys. Rev. Lett. **102**, 164801 (2009); H. Kotaki, I. Daito, M. Kando, Y. Hayashi, K. Kawase, T. Kameshima, Y. Fukuda, T. Homma, J. Ma, L.-M. Chen, T. Z. Esirkepov, A. S. Pirozhkov, J. K. Koga, A. Faenov, T. Pikuz, H. Kiriyama, H. Okada, T. Shimomura, Y. Nakai, M. Tanoue, H. Sasao, D. Wakai, H. Matsuura, S. Kondo, S. Kanazawa, A. Sugiyama, H. Daido, and S. V. Bulanov, *ibid.* **103**, 194803 (2009).

[8] S. Bulanov, N. Naumova, F. Pegoraro, and J. Sakai, Phys. Rev. E **58**, R5257 (1998); H. Suk, N. Barov, J. B. Rosenzweig, and E. Esarey, Phys. Rev. Lett. **86**, 1011 (2001).

[9] C. G. R. Geddes, K. Nakamura, G. R. Plateau, Cs. Tóth, E. Cormier-Michel, E. Esarey, C. B. Schroeder, J. R. Cary, and W. P. Leemans, Phys. Rev. Lett. **100**, 215004 (2008); K. Schmid, A. Buck, C. M. S. Sears, J. M. Mikhailova, R. Tautz, D. Herrmann, M. Geissler, F. Krausz, and L. Veisz, Phys. Rev. ST Accel. Beams **13**, 091301 (2010); J. Faure, C. Rechatin, O. Lundh, L. Ammoura, and V. Malka, Phys. Plasmas **17**, 083107 (2010).

[10] D. Umstadter, J.-K. Kim, and E. Dodd, Phys. Rev. Lett. **76**, 2073 (1996); "Method and apparatus for generating and accelerating ultrashort electron pulses," U.S. Patent No. 5,789,876.

[11] M. Chen, Z.-M. Sheng, Y.-Y. Ma, and J. Zhang, J. Appl. Phys. **99**, 056109 (2006).

[12] A. Pak, K. A. Marsh, S. F. Martins, W. Lu, W. B. Mori, and C. Joshi, Phys. Rev. Lett. **104**, 025003 (2010); C. McGuffey, A. G. R. Thomas, W. Schumaker, T. Matsuoka, V. Chvykov, F. J. Dollar, G. Kalintchenko, V. Yanovsky, A. Maksimchuk, K. Krushelnick, V. Y. Bychenkov, I. V. Glazyrin, and A. V. Karpeev, **104**, 025004 (2010).

[13] J. S. Liu, C. Q. Xia, W. T. Wang, H. Y. Lu, C. Wang, A. H. Deng, W. T. Li, H. Zhang, X. Y. Liang, Y. X. Leng, X. M. Lu, C. Wang, J. Z. Wang, K. Nakajima, R. X. Li, and Z. Z. Xu, Phys. Rev. Lett. **107**, 035001 (2011); B. B. Pollock, C. E. Clayton, J. E. Ralph, F. Albert, A. Davidson, L. Divol, C. Filip, S. H. Glenzer, K. Herpoldt, W. Lu, K. A. Marsh, J. Meinecke, W. B. Mori, A. Pak, T. C. Rensink, J. S. Ross, J. Shaw, G. R. Tynan, C. Joshi, and D. H. Froula, **107**, 045001 (2011).

[14] M. Chen, E. Esarey, C. B. Schroeder, C. G. R. Geddes, and W. P. Leemans, Phys. Plasmas **19**, 033101 (2012).

[15] N. Bourgeois, J. Cowley, and S. M. Hooker, Phys. Rev. Lett. **111**, 155004 (2013).

[16] B. Hidding, G. Pretzler, J. B. Rosenzweig, T. Königstein, D. Schiller, and D. L. Bruhwiler, Phys. Rev. Lett. **108**, 035001 (2012).

[17] Y. Xi, B. Hidding, D. Bruhwiler, G. Pretzler, and J. B. Rosenzweig, Phys. Rev. ST Accel. Beams **16**, 031303 (2013).

[18] J.-L. Vay, D. P. Grote, R. H. Cohen, and A. Friedman, Computational Science and Discovery **5**, 014019 (2012).

[19] V. S. Popov, Physics Uspekhi **47**, 855 (2004).

[20] M. Chen, E. Cormier-Michel, C. Geddes, D. L. Bruhwiler, L. L. Yu, E. Esarey, C. B. Schroeder, and W. P. Leemans, J. Comput. Phys. **236**, 220 (2013).

[21] C. Benedetti, C. B. Schroeder, E. Esarey, and W. P. Leemans, Phys. Plasmas **19**, 053101 (2012).

[22] A. Dubietis, R. Butkus, and A. P. Piskarskas, IEEE J. Sel. Top. Quant. Electron. **12**, 163 (2006).